Acta Materialia 105 (2016) 52–58

Contents lists available at ScienceDirect

Acta Materialia

journal homepage: www.elsevier.com/locate/actamat

Full length article

Synchrotron analysis of toughness anomalies in nanostructured bainite

L.C.D. Fielding [a], N.G. Jones [a], J. Walsh [b], S. Van Boxel [b], M.S. Blackmur [b], P.D. Lee [b], P.J. Withers [b], H.J. Stone [a, *], H.K.D.H. Bhadeshia [a]

[a] Department of Materials Science and Metallurgy, University of Cambridge, 27 Charles Babbage Road, Cambridge CB3 0FS, UK
[b] School of Materials, University of Manchester, Oxford Road, Manchester M13 9PL, UK

ARTICLE INFO

Article history:
Received 2 October 2015
Received in revised form
13 November 2015
Accepted 15 November 2015
Available online xxx

Keywords:
Bainitic steel
Synchrotron diffraction
Charpy impact test
Toughness

ABSTRACT

High-resolution synchrotron X-ray diffraction has been used to characterise the notch root regions of Charpy impact test specimens of a superbainitic steel, both before and after loading. The changes in the volume fraction of austenite induced by the application of a three-point-bending load were quantified. Analysis of diffraction peak shifts revealed the extent of residual tensile and compressive strains present due to both machining and an applied load. The results lend support to the hypothesis that the comparatively low energies absorbed during Charpy impact testing of superbainitic steels, <7 J, are due to the formation of stress-induced martensite at the notch root, prior to crack initiation.

© 2015 Acta Materialia Inc. Published by Elsevier Ltd. This is an open access article under the CC BY license (http://creativecommons.org/licenses/by/4.0/).

1. Introduction

Nanostructured bainitic steels, comprised of <10 nm-thick bainitic sheaves distributed within carbon-enriched austenite, have some exceptional properties with yield strengths of up to 1500 MPa and elongations in excess of 20% [1]. Critically, these properties can be achieved in thick sections following relatively low-temperature heat treatments, without the need for rapid cooling or severe deformation [2–4]. The benefits offered by these alloys are such that they are now produced commercially.

However, it has been asserted that the Charpy impact toughness of these nanostructured steels is unexpectedly small when compared with their fracture toughness, K_{1C} [1]. For alloys of almost identical chemical composition and heat treatment, the Charpy energy at room temperature is reported to be only 4–7 J whereas K_{1C} has been measured in the range 28–32 MPa $m^{1/2}$ [5,6]. However, it remains the case that most of the data published do not contain both measures of toughness on the same alloy [5,7–12]. In general, when comparisons are made across nanostructured bainite of different compositions, the range of Charpy energies remains within 4–7 J, whereas the fracture toughness ranges from 28 to 55 MPa $m^{1/2}$. Recently, a direct comparison has been made in a fast-transforming superbainitic steel, which again showed Charpy energies and fracture toughnesses in these ranges [13]. This apparent disparity may be a result of the different sample geometries required by the two tests; in a Charpy test a blunt notch is used, whereas a K_{1C} specimen has a sharp crack. During an impact test, the stress-affected volume at the Charpy notch root is more extensive, as a result of the larger root radius, compared with an equivalent K_{1C} sample. It has been hypothesised that this creates a large region containing brittle martensite prior to crack initiation [1]. This is supported by observations of martensite on the fracture surfaces of bainitic steels following Charpy impact testing using X-ray diffraction [14] and transmission electron microscopy [15]. As a result, when the sample fails, it does so in a brittle manner. Since a K_{1C} sample contains a sharp crack, the corresponding stress-affected region is smaller than the austenitic regions, such that any martensite formed will remain surrounded by retained austenite. Understanding such behaviour is important for assessing the relevance of the Charpy toughness results from these alloys, and to work towards controlling the toughness on the basis of phase-transformation theory.

During a Charpy impact test, the specimen is subject to rapid three-point-bend loading. By applying a three-point-bend at low strain-rates, it is possible to recreate the loading conditions that exist at the notch prior to failure, but not the consequences of

* Corresponding author.
E-mail address: hjs1002@cam.ac.uk (H.J. Stone).

http://dx.doi.org/10.1016/j.actamat.2015.11.029
1359-6454/© 2015 Acta Materialia Inc. Published by Elsevier Ltd. This is an open access article under the CC BY license (http://creativecommons.org/licenses/by/4.0/).

strain-rate. High-resolution synchrotron X-ray diffraction provides a means of accurately measuring the lattice distortion and phase fraction distribution in the vicinity of the notch, before and after loading. It was therefore the aim of the present study to investigate, using synchrotron techniques, the response of the material at the notch root to an applied stress.

2. Experimental methods

The chemical composition of the alloy used is shown in Table 1. Compared to other nanostructured bainitic steels, this alloy has a relatively low silicon concentration for better continuous casting quality and a low manganese concentration to accelerate the bainitic transformation [16]. The samples were austenitised at 930 °C for 1 h in a tube furnace under an argon atmosphere and subsequently isothermally transformed at 200 °C for 96 h, followed by water quenching.

Microstructural characterisation of the heat treated material was performed by transmission electron microscopy (TEM) using a JEOL 200CX operated at 200 keV. Electron transparent samples were produced by twin-jet polishing with a solution of 15% perchloric acid in ethanol at 7.5 °C and a voltage of 26 V.

Sub-size Charpy specimens with dimensions of 10 mm × 7.5 mm × 55 mm were prepared from 8 mm-thick plate according to the EN 10045-1 standard. The specimens were heat treated as blanks before being sent for final machining. The Charpy specimens were oriented with the notch in the rolling direction, due to the presence of strong banding in the as-received plate.

Bend tests were carried out using an 100 kN servo hydraulic machine, with a support span of 40 mm and a displacement rate of 0.5 mm min^{-1}. Under these conditions, the failure load was found to be ~10 kN. Subsequent samples were loaded to 8 kN and then unloaded, allowing the intact notch root region to be examined. These samples were sliced lengthwise into 2 mm-thick sections using electro-discharge machining. Similar sections were taken from unstressed Charpy samples. The surface of each slice was ground and polished using SiC paper (800-grade to 4000-grade).

High energy X-ray diffraction was performed on the I15 beamline at the Diamond Light Source in Oxford, UK, using a monochromatic X-ray beam with dimensions of 70 × 70 μm and a wavelength of 0.16557 Å. Each diffraction pattern was captured in transmission over 40 s using a flat, 2-D Perkin–Elmer detector mounted perpendicular to the incident beam. In the unstressed sample, a region roughly 1 × 1 mm in size was mapped by taking spectra over a fine grid (step size 70 μm) close to the notch root, and a coarser grid (step size 100 μm) further from the notch root. A step size of 70 μm was used over the full scan region (2 × 1 mm) underneath the stressed notch, and a step size of 100 μm was used to scan a 1 × 1 mm un-notched region. In the case of the unstressed notch, only half the notch region was scanned, due to time constraints. A lanthanum hexaboride (LaB_6) powder standard was used as a calibrant to refine the instrument parameters. A schematic illustration of the experimental setup is shown in Fig. 1.

Data were recorded as 2-D images and were integrated azimuthally to convert to 1-D intensity *versus* 2θ data using Fit2D [18–20]. This analysis was considered valid as a previous study of the present alloy has shown that it is not significantly textured [13].

Quantitative phase analysis was performed using Rietveld refinement with Bruker TOPAS v.4.2 software. The volume fractions of the austenite and ferrite were obtained by fitting to the first four reflections of each phase. By using multiple peaks, the influence of any textural effects upon the refinement results was minimised [21]. Although it is expected that martensite forms in the notch region, the quantities were too small to be characterised unambiguously and it was not possible to separate the ferrite peaks reliably into two distinct phases. Therefore, only austenite and ferrite were assumed to be present in the diffraction data analysis.

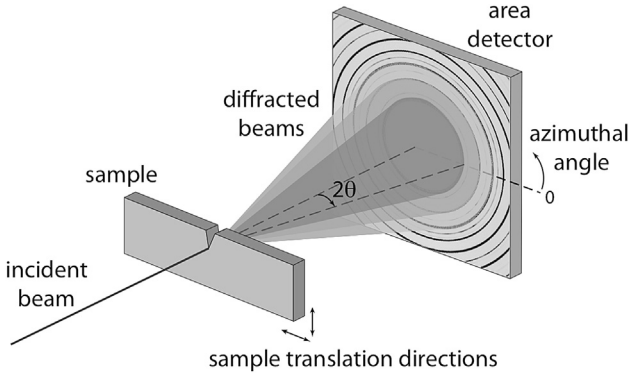

Fig. 1. Illustration of the experimental setup, adapted from Ref. [17].

The orientation dependence of the lattice distortion was evaluated through fitting of single (and dual, in the case of the $\{111\}_\gamma$/$\{110\}_\alpha$ reflections) peaks with a Voigt function from 10° azimuthal segments taken at the cardinal points (azimuthal angles of 0°, 90°, 180° and 270°) of the Debye-Scherrer rings using Fit2D, and peak fits were performed with Wavemetrics Igor Pro. The *hkl*-specific strain was calculated as $\varepsilon_{hkl} = \Delta d/d_i$, where d_i was taken as an average of the *d*-spacings measured in each sample away from the notch. Similarly, the average lattice strain, ε_{av} was obtained as $\varepsilon_{av} = \Delta a/a_i$, where a_i is the average lattice parameter obtained from the Rietveld refinement of multiple peaks. Obtaining the average lattice strain in this way has been shown previously to provide an effective measure of the macrostrain, avoiding the effects of type II stresses [22].

3. Results and discussion

3.1. Microstructure

A representative TEM micrograph of the alloy following isothermal transformation at 200 °C for 96 h and water quenching is shown in Fig. 2. The microstructure comprised nanoscale bainitic plates with a mean plate thickness of 57 ± 3 nm, as determined from over 800 individual measurements [13]. Whilst still in the nanoscale range, the observed plate thickness is coarser than that reported for other superbainitic steels. This may be a consequence of the lower concentrations of alloying additions, which provide less solid solution strengthening of the austenite and thereby allow coarser plates to form [23]. In addition, the lower silicon content of this alloy, compared with other nanostructured bainitic steels, does not fully suppress the formation of cementite within the microstructure. Detailed analysis identifying the presence of cementite in

Table 1
Chemical composition of alloy, wt%.

C	Si	Mn	Ni	Cr	Mo	Al	Cu	Sn	N	P	S
0.82	0.71	1.30	0.02	0.9	0.2	0.033	0.02	0.004	0.007	0.01	0.003

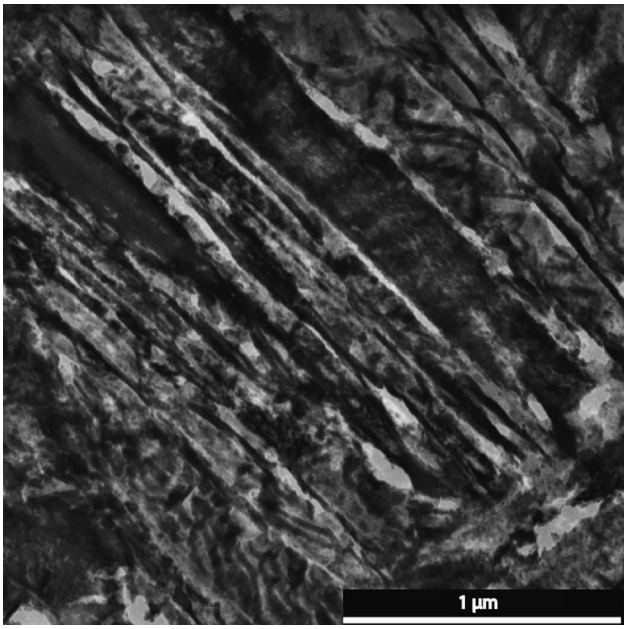

Fig. 2. Transmission electron micrograph of the alloy in the heat treated condition.

the alloy in this condition can be found in Ref. [13].

3.2. Peak fitting

Fig. 3 shows an example of a diffraction spectrum obtained from a 10° azimuthal segment. Strong reflections from the ferrite and weaker reflections from the retained austenite phases were observed. Despite the high signal to noise ratio, characteristic of synchrotron radiation, no reflections corresponding to cementite could be discerned, consistent with the low volume fraction and fine scale nature of this phase. Inset are shown magnified regions around the austenite 200 and ferrite 200 reflections. Single peak fits of the 10° azimuthal segments confirmed that all of the 200 ferrite reflections could be described extremely well using a single Voigt function, despite previous work suggesting that superbainitic ferrite is better modelled as a tetragonal structure [24,25]. Critically, it was noted that a tetragonal model was required to successfully describe the peak profiles obtained when the Debye Scherrer rings were azimuthally integrated around the full 360°. This observation can be attributed to the presence of residual strains within the diffracting volume. Such residual strains arise as a result of prior mechanical processing, such as rolling, and alter the *d*-spacing of each *hkl* reflection with azimuthal angle, inline with the processing geometry. As a consequence, full 360° azimuthal integration will result in an asymmetric peak shape, whilst smaller azimuthal integrations, such as those used in the later analysis, avoid this effect, producing symmetric peaks.

In contrast, the austenite reflections displayed a visible asymmetry even in the azimuthally segmented data (Fig. 3a). This is typical of superbainitic material, in which austenite is present in both 'film' and 'blocky' forms with an associated bimodal carbon distribution that results in an asymmetric peak shape [14,26,27]. Nevertheless, single peak fitting proved to be sufficiently accurate and reliable for determining peak width and position in the present case.

One indication of martensitic transformation is an observable shift of the austenite peaks to lower angles. It is expected that the austenite with lower carbon content is less stable and will therefore transform preferentially. However, the presence of residual strain at the notch root of both samples precluded the possibility of unambiguously identifying any peak shifts of this nature. Similarly, directly, beneath the notch root the intensities of the austenite peaks were lower than that observed elsewhere in the sample. This behaviour is consistent with a phase transformation having taken place.

3.3. Phase fractions

The results of the phase fraction analysis are presented in Fig. 4 as a contour plot of the volume fraction of retained austenite in the region 1 × 2 mm directly beneath the notch. The notch root is located at $x = 0$, $y = 0$. It is evident that the volume fraction of retained austenite at the notch root of a Charpy sample is significantly reduced following the application of a three-point bending load. The retained austenite content of the specimen varies only at the very base of the notch, over a vertical distance of 70 μm,

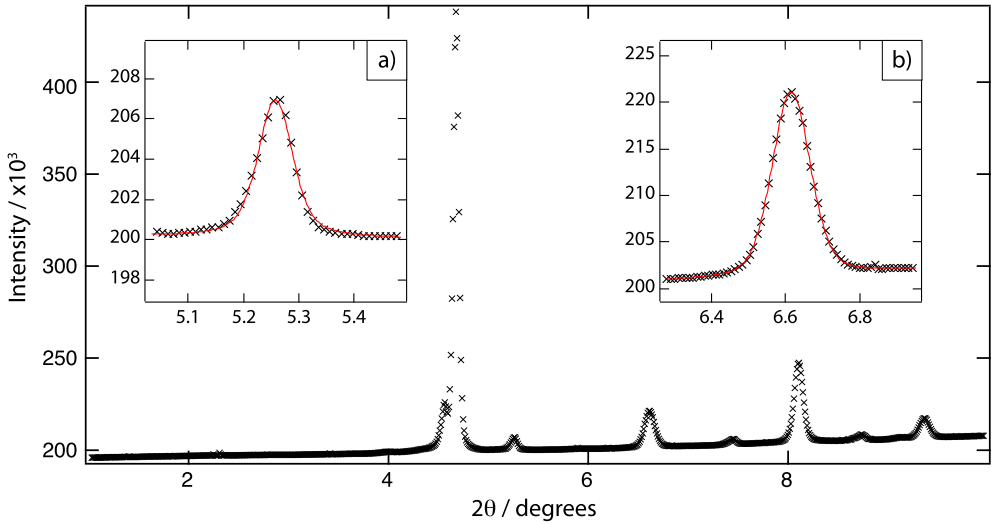

Fig. 3. An example diffraction spectrum taken at a distance remote from the stressed notch. These data were taken from a 10° azimuthal segment around an azimuthal angle of 90°. Examples of single Voigt peak fits for (a) austenite 200 peak; (b) ferrite 200 peak are inset. Note the excellent fit in the case of ferrite, and the clear asymmetry in the case of austenite.

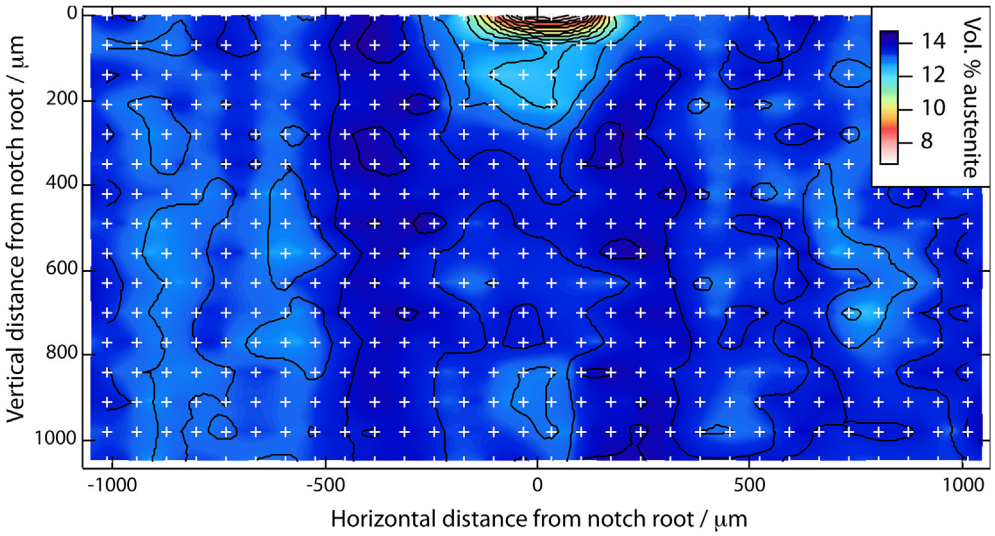

Fig. 4. Retained austenite content mapped in the notch root region of a stressed sample. The measurement positions are identified by white cross markers.

corresponding to the width of the beam. The size of the affected region below the notch is approximately 70 μm deep by 400 μm wide. This is a fairly large area and is consistent with the expectation that stressed Charpy specimens develop a transformed notch region of significant size prior to crack initiation.

Fig. 5 shows the volume fraction of retained austenite immediately below the notch as a function of distance in three samples: a notched and stressed sample; a notched sample not subjected to stress; and an un-notched sample. The data indicate that there is a reduction in the retained austenite content, even at the root of an unstressed notch, albeit to a lesser extent than in the sample that had been subjected to an applied stress. The effects of machining, which in this case was performed after heat treatment in order to avoid decarburisation effects, are evident. The implication is that the microstructure of the notch root region in such samples may be altered and embrittled if the notch is machined after heat treatment has been carried out. It should therefore be possible to improve the results of a Charpy toughness test in this material by ensuring the notch is machined prior to heat treatment. This result also raises the question of whether machining may have similar effects upon other types of test specimen.

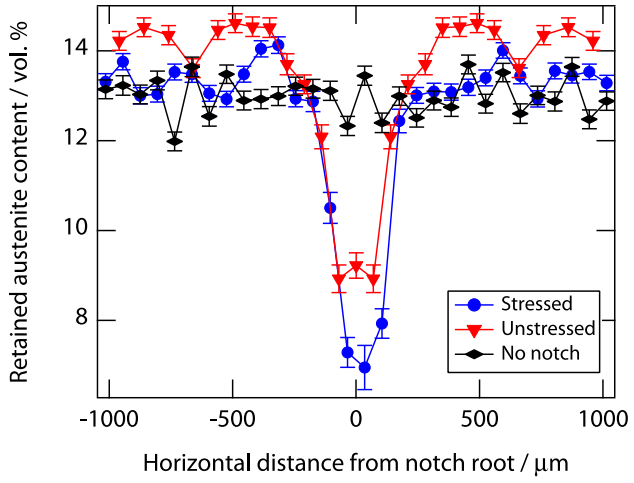

Fig. 5. Retained austenite content in three different specimens: notch stressed, notch unstressed and no notch. The data represent horizontal line-scans taken directly below the notch root. Note that the data for the unstressed notch were obtained by scanning only half the notch root region and have been reflected about $x = 0$; the plot of that data is therefore symmetrical.

While synchrotron diffraction successfully showed clear changes due to both applied stress and machining in these samples, the disadvantage of this approach is the lack of repeat testing. Synchrotron beamtime is limited and it was therefore not possible to take notch measurements from more than one of each kind of sample during this study, or to repeat any of the individual measurements. Therefore, the results presented here provide no indication of sample-to-sample variation. For completeness, it would be desirable to measure the effect of machining and stressing on several samples to get an impression of the inherent variability of the data. However, it is encouraging that Fig. 5 shows reasonable retained austenite contents with increasing distance from the notch in all three samples.

3.4. Strain

Although the observed phase changes appear to be confined to a limited region directly below the notch, strain analysis revealed that the effects of notch machining and applied stress extended further into the material. Strain maps of the region below the stressed notch are presented in Fig. 6a and b, which were generated from the data obtained from the 10° azimuthal segments taken around azimuthal angles of 0° and 90°. The strain maps indicate that residual compressive strains exist in the horizontal direction, perpendicular to the direction of the notch, and tensile strains exist in the vertical direction, parallel to the direction of the notch. Peak compressive strains of the order of -8×10^{-3} were seen at the notch root parallel to the direction of the notch, consistent with the yield stress of the material. The strains immediately below the notch are balanced by a region of opposing strain deeper into the specimen, presumably generated as the surrounding material elastically deformed to accommodate the plastic strain induced in the surface layers. It is likely that this deformation induced the transformation to martensite below the notch.

The distribution of strain that exists as a function of distance from the notch is shown in Fig. 7 for all three samples. In this figure, the maximum tensile and compressive strains in both the stressed and unstressed samples are virtually identical, and are present over similar distances. This indicates that the presence of residual strains

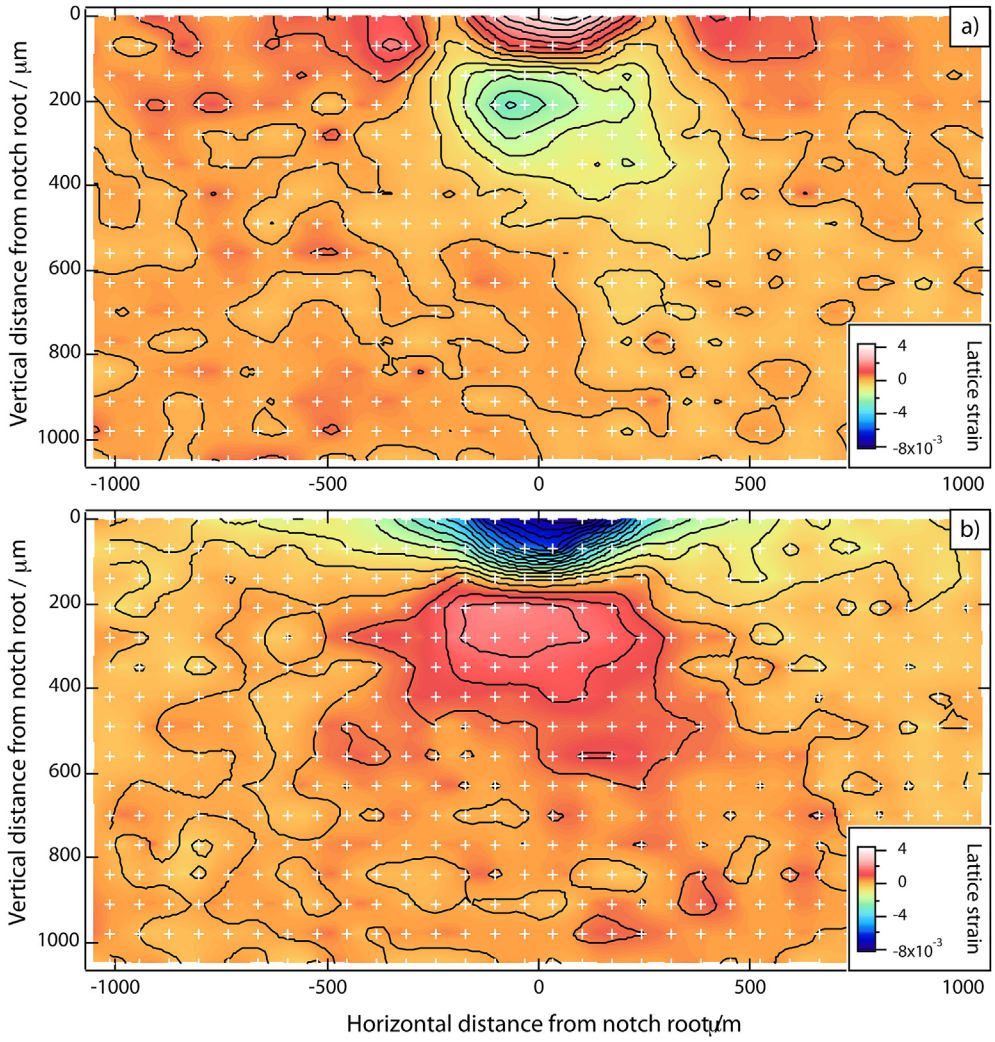

Fig. 6. Average lattice strain measured in the stressed sample, taken from azimuthal segments around azimuthal angles of (a) 0° (horizontal strain, perpendicular to the notch) and (b) 90° (vertical strain, parallel to the notch) around the diffraction ring. The measurement positions are identified by white cross markers.

is primarily a result of the notch machining process. However, the strain in the stressed sample persists over a slightly larger region; a disparity that is likely accounted for by the applied stress.

It is interesting to note that the tensile strains are generally lower than the compressive strains in these samples, evident from Fig. 7a and b. This may be a consequence of stress triaxiality and Poisson effects, which so far have not been considered in the analysis. The tensile strains are roughly half the compressive strains at each measurement position. A difference of 0.3 would indicate a simple uniaxial stress relationship between the two. This implies that a triaxial, or at least biaxial, stress distribution exists in the samples. This is not straightforward to quantify, however, since by slicing the original Charpy test pieces some stresses will have been relaxed, so the results obtained are not representative of the original strain distribution.

A second factor that is likely to have affected the stress distributions is the martensitic phase transformation. Martensite is formed by a displacive transformation, which is accompanied by both a shear strain and a volume increase. The data in Fig. 5 indicate that 4–6% of the material in the notch root region has transformed to martensite. If this material is sufficiently constrained, the volume change associated with the transformation would likely generate compressive strains. Such strains would have the effect of reducing the tensile strains present in the vertical direction as well as reinforcing the compressive strains in the horizontal direction. However, the magnitude of this effect is not easily determined, as the shear component of the transformation and the associated variants formed may preferentially relieve stresses in a particular direction. Nevertheless, the tensile strain plotted in Fig. 7a does show a sudden drop at the same position where martensite is first observed in Fig. 5, suggesting that the two features are linked.

The *hkl*-specific lattice strains in the stressed sample are plotted in Fig. 8. These traces follow the expected behaviour, insofar as the strain in the majority of directions matches closely the average strain shown in Fig. 7. Close to the notch, the strains in the [200] direction are significantly larger. In general, when such strains vary according to *hkl* reflection, it can be an indication of elastic and plastic anisotropy of the material and the occurrence of intergranular strains [28]. In BCC structures, the {200} reflection corresponds to the most compliant family of grains and is expected to exhibit the highest strain for a given applied stress [28]. This is consistent with what is seen in Fig. 8. The diffraction elastic constants for the other three reflections are very similar [28], although some small differences are evident in the measured strains, which suggests that only minor intergranular strains exist in those directions. In particular, it is only in the region very close to the notch

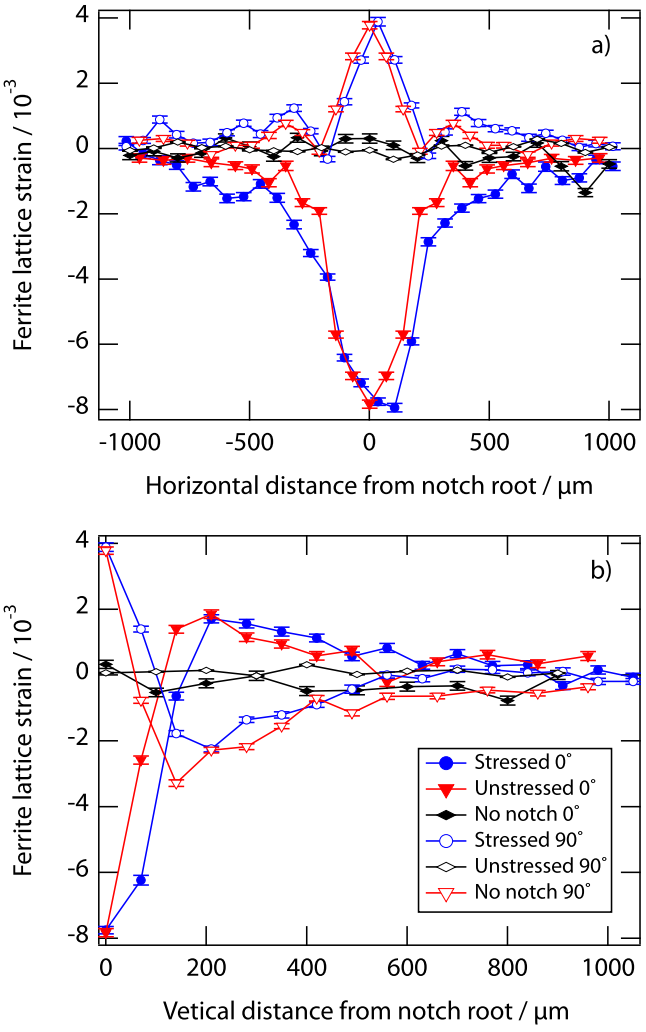

Fig. 7. Average lattice strain measured in the stressed sample, taken from azimuthal segments around azimuthal angles of 0° (horizontal strain) and 90° (vertical strain) around the diffraction ring. The data represent (a) horizontal and (b) vertical linescans. The data for the unstressed sample were taken over half the notch only, resulting in a symmetrical plot.

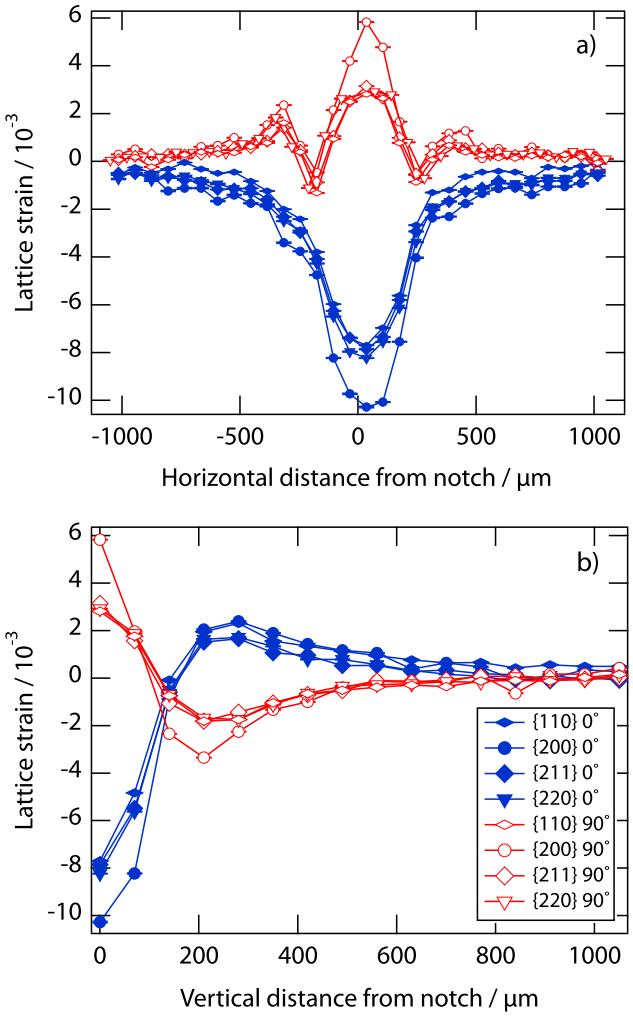

Fig. 8. ε_{hkl} measured in the stressed sample. The data represent (a) horizontal and (b) vertical linescans.

root where this *hkl* deviation occurs. Further from the notch, the measured strain is not *hkl* dependent, so any plasticity in this sample must exist over a small region at the notch root only. Additionally, Fig. 8 highlights that there are no significant intergranular stresses present in this area and that the *hkl* strain distribution can be explained by elastic anisotropy of the material alone.

The inhomogeneous strains associated with plasticity and phase transformation may lead to changes in peak width. In this particular case, broadening may also be indicative of increased tetragonality, defined by the ratio of the ferritic unit cell lattice parameters, *c*/*a*. The full width half maxima (FWHM) of various peaks, calculated from single peak fits of an azimuthally segmented data, corresponding to a region of compressive stress, are presented in Fig. 9. In addition to data from ferrite peaks, FWHM measurements were obtained from the austenite {200} peak. In all cases, a decrease in peak width was observed close to the notch, over an area corresponding to that affected by the residual strain. While increased peak width can be associated with a change in dislocation density encountered with plastic strains, decreases in peak width may be a consequence of the removal of type III strains, as was seen for 304-grade stainless steel by Rahman et al. [29]. This is attributable to the formation of martensite in this region. The decrease in peak width near the notch cannot be attributed to the increased volume fraction of martensite alone, as the slight differences between the lattice parameters of the ferrite and martensite would be expected to result in an apparent broadening of the diffraction peaks associated with the ferritic material.

4. Conclusions

High-resolution synchrotron diffraction has revealed, for the first time, the changes that occur at the notch root of a superbainitic Charpy sample subjected to three-point-bend loading. The aim was to discover the extent to which the austenite undergoes a transformation to martensite due to the intensified stresses in this region.

A marked decrease was observed in the volume fraction of residual austenite present at the notch root of a sample that had been stressed. Furthermore, a similar, but weaker, reduction in austenite content was seen in the notch region of an unstressed sample, indicating that the austenite in this alloy may have undergone martensitic transformation during machining.

The influence of machining was further highlighted by the presence of residual strains in an extensive region around the

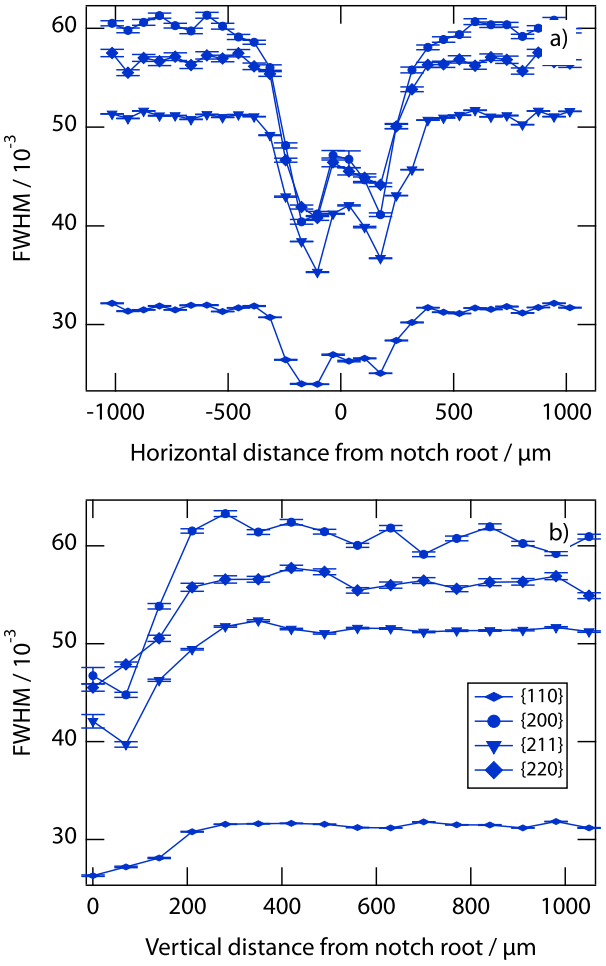

Fig. 9. Full width half maxima measured from the {110}, {200}, {211} and {220} reflections from the ferritic material in the stressed sample, from an azimuthal segment taken around an azimuthal angle of 0°. The data represent (a) horizontal and (b) vertical linescans.

notch. These strains were highly directional and extended much further into the sample than the freshly-formed martensite. Differences between the elastic strains measured in grains in different orientations were seen to be consistent with the elastic anisotropy of this material.

Acknowledgements

The authors are grateful to Prakash Srirangam Venkata and Bernard Ennis for their valuable contribution to the synchrotron work; to Diamond Light Source (Oxford) for access to the synchrotron facilities (under experiment EE8564); to Tata Steel UK and the Engineering and Physical Sciences Research Council of the UK for financial support (under EP/H500375/1 and EP/I02249X/1). The original research data is available at https://www.repository.cam.ac.uk/handle/1810/252605.

References

[1] H.K.D.H. Bhadeshia, Nanostructured bainite, Proc. R. Soc. A 466 (2010) 3–18.
[2] F.G. Caballero, H.K.D.H. Bhadeshia, K.J.A. Mawella, D.G. Jones, P. Brown, Very strong low temperature bainite, Mater. Sci. Technol. 18 (2002) 279–284.
[3] F.G. Caballero, H.K.D.H. Bhadeshia, Very strong bainite, Curr. Opin. Solid State Mater. Sci. 8 (2004) 251–257.
[4] H.K.D.H. Bhadeshia, The first bulk nanostructured metal, Sci. Technol. Adv. Mater. 14 (2013), 014202.
[5] P.M. Brown, D.P. Baxter, Hyper-strength bainitic steels, New Orleans, LA, USA, in: Proc. Conf. MS&T 2004, 2004, pp. 433–438 (TMS/ASM).
[6] C. Garcia-Mateo, F.G. Caballero, Ultra-high-strength bainitic steels, ISIJ Int. 45 (2005) 1736–1740.
[7] C. Garcia-Mateo, F.G. Caballero, H.K.D.H. Bhadeshia, Mechanical properties of low-temperature bainite, Mater. Sci. Forum 500–501 (2005) 495–502.
[8] M.R. Zhang, H.C. Gu, Microstructure and properties of carbide free bainite railway wheels produced by programmed quenching, Mater. Sci. Technol. 23 (2007) 970–974.
[9] T.S. Wang, J. Yang, C.J. Shang, X.Y. Li, B. Zhang, F.C. Zhang, Microstructures and impact toughness of low-alloy high-carbon steel austempered at low temperature, Scr. Mater. 61 (2009) 434–437.
[10] F.G. Caballero, J. Chao, J. Cornide, C. Garcia-Mateo, M.J. Santofimia, C. Capdevila, Toughness deterioration in advanced high strength bainitic steels, Mater. Sci. Eng. A 525 (2009) 87–95.
[11] S.K. Putatunda, C. Martis, J. Boileau, Influence of austempering temperature on the mechanical properties of a low carbon low alloy steel, Mater. Sci. Eng. A 528 (2011) 5053–5059.
[12] M.N. Yoozbashi, S. Yazdani, T.S. Wang, Design of a new nanostructured, high-si bainitic steel with lower cost production, Mater. Des. 32 (2011) 3248–3253.
[13] L.C.D. Fielding, Understanding Toughness and Ductility in Novel Steels with Mixed Microstructures, PhD thesis, University of Cambridge, 2014.
[14] H.K.D.H. Bhadeshia, D.V. Edmonds, Bainite in silicon steels: a new composition-property approach, part 2, Metal. Sci. 17 (1983) 420–425.
[15] Y.T. Tsai, H.T. Chang, B.M. Huang, C.Y. Huang, J.R. Yang, Microstructural characterization of charpy-impact-tested nanostructured bainite, Mater. Charact. 107 (2015) 63–69 cited By 0.
[16] A.J. Rose, F. Mohammed, A.W.F. Smith, P.A. Davies, R.D. Clarke, Superbainite: laboratory concept to commercial product, Mater. Sci. Technol. 30 (9) (2014) 1094–1098.
[17] N.G. Jones, C.M. Ward-Close, P.M. Brown, D. Dye, An evaluation of the tensile properties of a supersaturated carbon layer via in situ synchrotron diffraction, Scr. Mater. 63 (2010) 85.
[18] A.P. Hammersley, ESRF internal report, ESRF97HA02T, "FIT2D: An introduction and overview", Tech. Rep. ESRF (1997).
[19] A.P. Hammersley, S.O. Svensson, M. Hanfland, A.N. Fitch, D. Häusermann, Two-dimensional detector software: from real detector to idealised image or two-theta scan, High. Press. Res. 14 (1996) 235.
[20] A.P. Hammersley, FIT2D v9.129 reference manual v3.1. ESRF Internal Report ESRF98HA01T, ESRF (1998).
[21] M.J. Dickson, The significance of texture parameters in phase analysis by X-ray diffraction, J. Appl. Crystallogr. 2 (1969) 176–180.
[22] M.R. Daymond, M.A.M. Bourke, R.B. von Dreele, B. Clausen, T. Lorentzen, Use of Rietveld refinement for elastic macrostrain determination and for evaluation of plastic strain history from diffraction spectra, J. Appl. Phys. 82 (1997) 1554–1562.
[23] N. Chester, H.K.D.H. Bhadeshia, Mathematical modelling of bainite transformation kinetics, J. Phys. IV, C5 7 (1997) 41–46.
[24] J.H. Jang, H.K.D.H. Bhadeshia, D.W. Suh, Solubility of carbon in tetragonal ferrite in equilibrium with austenite, Scr. Mater. 68 (2012) 195–198.
[25] C.N. Hulme-Smith, I. Lonardelli, A.C. Dippel, H.K.D.H. Bhadeshia, Experimental evidence for non-cubic bainitic ferrite, Scr. Mater. 69 (2013) 409–412.
[26] H.K.D.H. Bhadeshia, D.V. Edmonds, Bainite in silicon steels: a new composition-property approach, part 1, Metal. Sci. 17 (1983) 411–419.
[27] H.J. Stone, M.J. Peet, H.K.D.H. Bhadeshia, P.J. Withers, S.S. Babu, E.D. Specht, Synchrotron x-ray studies of austenite and bainitic ferrite, Proc. R. Soc. A 464 (2008) 1009–1027.
[28] M.T. Hutchings, P.J. Withers, T.M. Holden, T. Lorentzen, Introduction to the Characterization of Residual Stresses by Neutron Diffraction, Taylor and Francis, 2005.
[29] K.M. Rahman, N.G. Jones, D. Dye, Micromechanics of twinning in a twip steel, Mater. Sci. Engin. A 635 (2015) 133–142.